Dynamics of turbulence strongly influenced by buoyancy

James J. Riley[a)]
University of Washington, Seattle, Washington 98195

Stephen M. deBruynKops
University of Massachusetts, Amherst, Massachusetts 01003

(Received 22 April 2002; accepted 25 March 2003; published 6 June 2003)

The dynamics of quasi-horizontal motions in a stably stratified fluid have been simulated for Froude numbers of order 1, so that the flows are strongly affected by the stable density stratification, and for a range of Reynolds numbers. It is found that the horizontal scales of the motion grow continuously in time. The vertical scales decrease and the vertical shearing increases with time, maintaining the Richardson number of order 1, as suggested by Lilly [J. Atmos. Sci. **40**, 749 (1983)] and Babin *et al.* [Theor. Comput. Fluid Dyn. **9**, 223 (1997)]. Small-scale instabilities and turbulent-like motions are observed to occur in the high shearing regions, while the larger-scale motions appear to evolve somewhat independently of the Reynolds number. The results suggest that the larger-scale, quasi-horizontal motions would be a continuous source of smaller-scale turbulence until the local Reynolds number drops below a critical value, which is estimated. Finally, a Froude number based upon a vertical differential scale and used in previous scaling arguments and theories is estimated in terms of other parameters. [DOI: 10.1063/1.1578077]

I. INTRODUCTION

When turbulence occurs in the presence of stable density stratification, it often decays due to the lack of a continuous source of energy. Examples of this include turbulence due to the breakdown of a propagating internal wave (e.g., Andreassen *et al.*,[1] Lelong and Dunkerton,[2,3] Lombard and Riley,[4,5] Bouret-Aubertot *et al.*,[6] and Orlanski and Bryan[7]), and turbulence resulting from a local shear instability (e.g., Turner,[8] Smyth[9]). As the turbulence decays its time scale L/u' tends to increase compared to the local buoyancy period $2\pi/N$. [Here L is a length scale typical of the energy-containing range of the turbulence, u' a rms turbulence velocity, $N^2 = -(g/\overline{\rho})(d\overline{\rho}/dz)$ the square of the buoyancy frequency, g the acceleration due to gravity, and $\overline{\rho}(z)$ the ambient density field, with z the vertical coordinate.] The Froude number $F_L = 2\pi u'/NL$, a ratio of these two time scales, is a measure of the importance of the stratification in the turbulence dynamics. Often in a turbulent event the Froude number starts out as very large (indicating stratification effects are not important) but, at some point in time, as the turbulence time scale continues to increase, the Froude number becomes of order 1, and the effects of stratification become an important aspect of the turbulence dynamics. (See Riley and Lelong[10] for a review of flows strongly affected by stable density stratification.)

This stratification effect is observed, for example, in the turbulent wakes of objects moving horizontally through a stably stratified fluid. For example, Spedding *et al.*[11,12] have observed a dramatic change in the decay characteristics of the turbulence when F_L becomes of order 1 (at a time t measured from the passage of the object such that $Nt \sim 1$). At somewhat later times ($Nt \sim 10$), the visual structure of the flow changes as quasi-horizontal vortices, sometimes referred to as "pancake eddies," develop in the flow (e.g., Lin and Pao;[13] Spedding *et al.*[12]). Exacting studies of these eddies have been carried out and, in fact, their detailed structure is now well-known (Chomaz *et al.*;[14] Bonnier *et al.*;[15] Spedding *et al.*;[12] Bonnier and Eiff[16]). Similar dynamics are observed to occur in other laboratory flows, for example, when a jet is introduced into a stably stratified fluid (Flór and van Heijst;[17] Voropayev *et al.*[18–20]).

Recently Trieling and van Heijst[21] and Beckers *et al.*[22,23] have addressed the dynamics of monopoles and dipoles in strongly stratified fluids, which can be considered as simplified models for the vortices found at late times in wake experiments. Employing laboratory experiments and numerical simulation, in addition to the formation of dipoles from monopoles and their subsequent interactions, they found significant distortion of the dipoles at higher Reynolds numbers. They also determined that the vortices remained in approximate cyclostrophic adjustment, and that their strength was continuously eroded by momentum transport by molecular diffusion, mainly in the vertical direction. The latter fact is consistent with the importance of vertical shearing of the horizontal motions found in the laboratory experiments of Fincham *et al.*[24]

A number of theoretical studies have been carried out to address the regime in which stratification effects become important in turbulent flows. For example, Riley *et al.*[25] have suggested a scaling analysis, intended to hold when the Froude number becomes small, which splits the flow into internal waves and vortical modes, the latter having properties similar to the quasi-horizontal vortices observed in the laboratory. This work was generalized by McWilliams[26] to

a)Author to whom all correspondence should be addressed; electronic mail: rileyj@u.washington.edu

include rotating, stratified flows, and a number of implications drawn. Lelong and Riley[27] have examined a resonant interaction in which a vortex mode acts as a catalyst for the exchange of energy between two internal waves (see also Bartello,[28] Majda and Embid,[29] Embid and Majda,[30] and Warn[31]), and Plougonven and Zeitlin[32] have used asymptotic methods to examine the internal wave emission from a pancake-like vortex. More extensive mathematical approaches, including continuous distributions of energy with length scale, have been offered by Majda and Embid,[29] Babin *et al.*,[33] and Bartello,[28,34] again for the more general case of rotating, stratified flows. Godeferd and Cambon[35] have addressed this problem using the eddy-damped, quasi-normal, Markovian theory, while Hanazaki and Hunt[36] have employed rapid distortion theory to examine the importance of linear phenomena.

This strongly stratified regime has been directly addressed in a number of numerical experiments, e.g., Riley *et al.*,[25] Herring and Métais,[37] and Bartello.[28] In these cases, significant changes in the dynamics, compared to nonstratified cases, were observed to occur, such as the upscale transfer of energy in the horizontal scales, but the maintenance of smaller vertical scales. The strongly stratified regime was also observed in the later time decay in numerical simulations of decaying, stably stratified turbulence, e.g., Métais and Herring,[38] Gerz and Yamazaki,[39] Ramsden and Holloway,[40] Gerz *et al.*,[41] Holt *et al.*,[42] Jacobitz *et al.*,[43] and Kimura and Herring.[44] Recently Gourlay *et al.*[45] have studied wake decay in stratified and nonstratified fluids using high resolution direct numerical simulations. They found, in particular, that the late-time vortices could be formed from an initial mean wake profile with superimposed random noise, without the necessity for any coherent vortices being shed from an obstacle.

Lilly[46] suggested that, due to weak vertical coupling of the horizontal motions, the dynamics in this strongly stratified regime should admit the continued generation of smaller vertical scales; this implies that, at high enough Reynolds numbers, Kelvin–Helmholtz-type instabilities would continually develop, with the local (gradient) Richardson number remaining of order 1. He speculated that the resulting smaller-scale turbulence might act as an ''eddy viscosity'' to the much larger-scale motions. Based upon their mathematical analysis, Babin *et al.*[33] refer to the limit of high Reynolds number, no rotation, and strong stratification as the ''catastrophe limit,'' since they predict that in this limit vertical variability leads to unbounded vertical shearing, again implying the generation of smaller-scale turbulence. Billant and Chomaz[47] have shown that, in model problems with strong stable stratification, the quasi-horizontal flows can be subject to a ''zig-zag'' instability, again which could lead to smaller-scale turbulence. Billant and Chomaz[48] also developed scaling laws for strongly stratified flows which indicate that, if no vertical scale is imposed by initial or boundary conditions, the vertical length scale should behave as $L_V \sim u'/N$. Taking L_V to be the vertical differential length scale of the horizontal velocity, this supports the suggestion of Lilly.

There are a number of issues raised by these laboratory experiments, numerical simulations, and theoretical analyses. In particular it is suggested that, as the turbulence becomes strongly influenced by stratification, the flow will change character and new types of dynamics and pathways to instabilities will appear. These instabilities require the local Reynolds number to be sufficiently large. In the laboratory experiments and numerical simulations, however, the local Reynolds numbers tend to be somewhat low, especially by the time, for example, that the quasi-horizontal vortices develop. Therefore it is not clear how such results might scale up to the high Reynolds numbers often characteristic of atmospheric and oceanic turbulence.

The objective of this study is to address the dynamics of flows in the regime where stable stratification has become important, or even dominant. In particular, we test the predictions of Lilly and Babin *et al.* of the development of new pathways to instabilities in this regime, and furthermore test the sensitivity of these instabilities and subsequent motions to the local Reynolds number. The results allow estimates of the critical Reynolds number for the flow to remain turbulent, and give insight into the scalability to high Reynolds number of the laboratory experiments and numerical simulations. We study these flows using high resolution direct numerical simulations applied to flows initialized with quasi-horizontal motions in the strongly stratified regime. The simulations are initialized with ''Taylor–Green'' vortices[49] which, when properly oriented, possess some of the properties of the late-time, quasi-horizontal vortices observed in the laboratory. Simulations are performed at several Froude numbers and for a range of Reynolds numbers in order to determine the effects of these parameters on the resulting flow fields.

In Sec. II we describe the flow fields addressed, the initial conditions for the simulations, and the numerical methods. In Sec. III we present our numerical results. In Sec. IV we summarize and discuss our conclusions, as well as speculate on their implications.

II. METHODOLOGY

In the flows considered, the ambient stratification was taken to be constant, and hence N was constant, and there was no ambient current shear. The initial conditions for each simulation consisted of Taylor–Green vortices plus low-level noise. The Taylor–Green vortices were oriented with the velocity field horizontal, and were of the following mathematical form:

$$\mathbf{v} = \mathcal{U}\cos(\kappa z)[\cos(\kappa x)\sin(\kappa y), -\sin(\kappa x)\cos(\kappa y), 0].$$

Here $\mathcal{U}$ determines the velocity scale, and $\ell = 1/\kappa$ the length scale of this initial flow field. In the simulation results presented, velocities are nondimensionalized by $\mathcal{U}$, lengths with $\ell = 1/\kappa$, and time with $\ell/\mathcal{U}$. The Froude number and Reynolds number characterizing the simulations are defined as

$$F_\ell = \frac{2\pi\mathcal{U}}{N\ell}, \quad \mathrm{Re}_\ell = \frac{\mathcal{U}\ell}{\nu},$$

respectively. The noise was broad-banded, with a level of approximately 10% of the initial Taylor–Green vortex energy.

The density perturbation field was usually initialized to zero, so that density fluctuations only appeared due to the action of the flow field on the ambient density gradient. Some cases were run, however, with the initial density perturbation field in cyclostrophic adjustment with the velocity field. For the Froude numbers considered, however, this adjustment did not appreciably affect the overall results. Therefore only cases with the initial density perturbation field of zero are presented here.

The flow fields are assumed to satisfy the Navier–Stokes equations subject to the Boussinesq approximation (see, e.g., Phillips[50]), so that, with the nondimensionalization introduced above, the governing equations are

$$\frac{\partial \mathbf{v}}{\partial t}+\mathbf{v}\cdot\nabla\mathbf{v}=-\left(\frac{2\pi}{F_\ell}\right)^2\rho\mathbf{e}_z-\nabla p+\frac{1}{\mathrm{Re}_\ell}\nabla^2\mathbf{v},$$

$$\nabla\cdot\mathbf{v}=0,$$

$$\frac{\partial \rho}{\partial t}+\mathbf{v}\cdot\nabla\rho-w=\frac{1}{\mathrm{Re}_\ell \mathrm{Pr}}\nabla^2\rho.$$

Here $\mathbf{v}=(u,v,w)$ is the velocity vector, and ρ and p the density and pressure deviations from their ambient values. Also $\mathrm{Pr}=\nu/\mathcal{D}$ is the Prandtl number (or Schmidt number, depending on the case), with ν the kinematic viscosity and $\mathcal{D}$ the mass diffusivity, and $\mathbf{e}_z$ is a unit vector in the vertical (z) direction. In the following simulations, Pr is taken to be 1.0, close to its value for temperature in air, but far from its appropriate values for temperature or salinity in the ocean. The pressure has been scaled by the dynamic pressure, $\rho\mathcal{U}^2$, and the density using the ambient density gradient, i.e., it is scaled by $\ell|d\overline{\rho}/dz|$.

Riley *et al.*[25] and Lilly[46] introduced a unique decomposition of the flow field that, in the limit as $F_\ell\to 0$, separates the flow into vortical mode and internal wave components. [When an ambient (horizontal) current $\mathbf{U}(z)$ is present, it must also be included in the decomposition (Staquet and Riley[51]).] In analogy with Helmholtz's decomposition, Lilly pointed out that the velocity field could be written uniquely in terms of a three-dimensional stream function ψ and a velocity potential $\phi=\partial\alpha/\partial z$ as

$$\mathbf{v}=\mathbf{U}(z)+\mathbf{e}_z\times\nabla_H\psi+\nabla_H\phi-\mathbf{e}_z\nabla_H^2\alpha. \tag{1}$$

Here the subscript H denotes the horizontal component of the vector operator. The second term on the right-hand side represents the vortical mode component, while the third and fourth terms represent the internal wave component. For the Taylor–Green initialization, only the vortical mode component is present. These simulations will thus emphasize this component of the flow field.

Taylor–Green vortices have been used previously in direct numerical simulations. Brachet *et al.*[52] demonstrated that, without density stratification, the flow would develop into a close approximation to isotropic turbulence, but with Taylor–Green geometric symmetries. Riley *et al.*[53] found that, with very strong stratification ($F_\ell\ll 1$) and no noise applied, the flow would viscously decay as predicted analytically. With noise applied, however, the flow was found to be unstable, with length scales growing in the horizontal, but decreasing in the vertical. In these simulations, the density stratification was strong enough that the local Richardson numbers were never low enough that secondary instabilities of the type presented in the following developed. The results of these simulations with very strong stratification were completely consistent with the scaling analysis of Riley *et al.*[25] In the present simulations, low-level, broad-banded noise is added to the Taylor–Green vortices as initial conditions in order to both break the Taylor–Green symmetries and also to excite the instabilities observed by Riley *et al.*[53]

The initial Taylor–Green fields have some properties in common with the quasi-horizontal vortices observed in the laboratory. The initial flow is horizontal, with a horizontal vortex structure, but with variation in the vertical. Furthermore, the vortices are packed close enough to interact, as is especially the case in early vortex evolution in the laboratory experiments. Note that the vertical length scale ℓ is imposed by the initial conditions. As the flows develop in time, however, the differential vertical scale is selected by the flow dynamics.

Cases were simulated for the initial Reynolds numbers over the following range:

$$\mathrm{Re}_\ell=800,\ 1600,\ 3200,\ 6400.$$

The initial Froude number was chosen to be small enough that stratification effects were important, but not too small that they were dominate. The values chosen were

$$F_\ell=2,\ 4.$$

The flow field was taken to be square periodic in the horizontal directions, with (dimensional) periods $\mathcal{L}_H$ of either

$$\mathcal{L}_H=4\pi\ell,$$

or

$$8\pi\ell\quad(\ell=1/\kappa),$$

and also to be periodic in the vertical (z) direction, with (dimensional) periods $\mathcal{L}_V$ of either $2\pi\ell$ or $4\pi\ell$. It was found that, since the vertical scales did not grow but decreased in the simulations, as long as the vertical domain size was taken to be at least $2\pi\ell$, the problem was insensitive to this boundary condition. The boundary conditions in the horizontal direction were influential, however, since the horizontal scales of the flow continuously grow with time.

Pseudo-spectral numerical methods were used to treat spatial derivatives, with third-order Adams–Bashforth time stepping. A spherical wave-number truncation of approximately 15/16 $\kappa_{\max}$, with $\kappa_{\max}$ the maximum wave number in the discrete Fourier transforms, was used to eliminate the most damaging aliasing errors (Orszag and Patterson[54]). The momentum equation was time-stepped with the nonlinear term expressed in vorticity form, while an alternating time-step scheme was employed for the density equation in order to eliminate most of the aliasing errors (Kerr[55]).

Table I contains a list of the simulations discussed in the following, along with the corresponding values for the Reynolds and Froude numbers, the domain size, and the number of grid points in the x, y, and z directions (N_x, N_y, N_z), re-

TABLE I. List of numerical simulations.

Identifier	F_ℓ	Re_ℓ	$\mathcal{L}_H/\ell$	$\mathcal{L}_V/\ell$	N_x	N_y	N_z
F2R16	2	1600	4π	4π	256	256	256
F2R32	2	3200	4π	2π	512	512	256
F2R64	2	6400	4π	2π	512	512	256
F4R8	4	800	4π	4π	256	256	256
F4R16	4	1600	4π	2π	256	256	128
F4R32	4	3200	4π	2π	512	512	256
F4R64	4	6400	4π	4π	512	512	512

spectively. Note that several cases with $F_\ell=2$ have been computed; their results are entirely consistent with the results presented in the following for the cases with $F_\ell=4$ and will not be emphasized. Furthermore, several additional cases were run, changing the domain size and/or the numerical resolution, in order to test the accuracy and robustness of the results presented. The results of these additional runs were consistent with those presented in the following, and so will not be discussed.

III. SIMULATION RESULTS

A. General features

A general idea of the flow dynamics can be seen by examining the stream function ψ defined in Eq. (1), and representing the vortical mode portion of the flow field. As will be established in the following, the vortical mode field is dominant for this flow, so that ψ gives a good approximation to the flow field, especially for the purpose of qualitative description of the flow.

In Fig. 1 is given three-dimensional gray scale contour plots of ψ for the initial conditions and for a later point in time ($t=20$) for the case with $F_\ell=4$, $\mathrm{Re}_\ell=3200$. Other simulations display qualitatively similar results. Note that, with the nondimensionalization discussed in Sec. II, the buoyancy period is $(2\pi/N)/(\ell/\mathcal{U})=F_\ell=4$ in this case. In the upper plot in the figure (for $t=0$) the spatial periodicity of the initial Taylor–Green field is evident, with the same wavelength in both the horizontal and vertical directions. As this flow develops in time, it is seen in the lower plot (at $t=20$) that the length scales in the horizontal direction are growing, while those in the vertical direction are decreasing.

Another view of these features can be seen in Fig. 2, in which are presented contours of ψ at $t=20$ at two different horizontal cross sections for the same case as in Fig. 1. The two cross sections were chosen just above and just below a plane of symmetry ($z=2\pi$) in the Taylor–Green field. Without any noise added to the flow field, ψ would be identical in these two planes.

The growth of length scales in the horizontal is clearly evident from the figures. As suggested by the heuristic arguments of Lilly,[46] these two layers evolve in a noticeably different manner, so that their appearance at $t=20$ is somewhat different. As a result of the growing dissimilarity in the flow fields for any two nearby but vertically separate points at the same horizontal location, an increase in the vertical shearing of the horizontal motions would be expected.

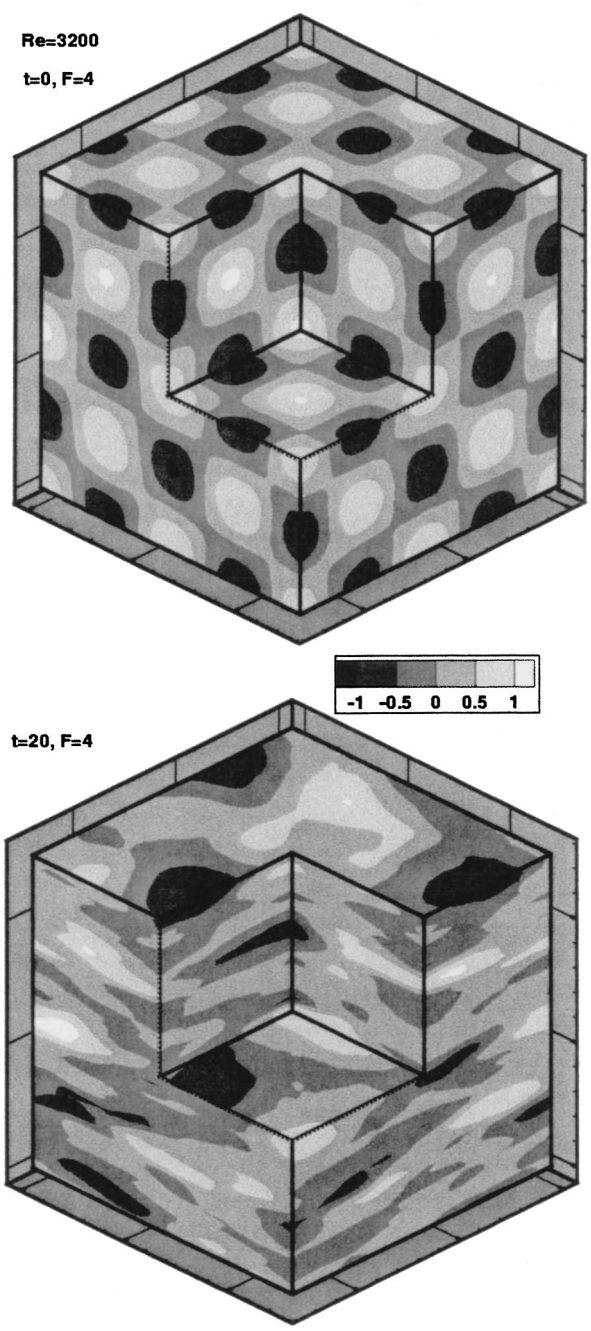

FIG. 1. Three-dimensional contour plots of the stream function ψ for the case with $F_\ell=4$, $\mathrm{Re}_\ell=3200$ at $t=0$ (upper plot), and $t=20$ (lower plot).

In Fig. 3 is given a plot of the horizontally averaged square of the shear versus z, i.e.,

$$\left\langle \left(\frac{\partial u}{\partial z}\right)^2+\left(\frac{\partial v}{\partial z}\right)^2 \right\rangle_H,$$

where $\langle\cdot\rangle_H$ denotes horizontal averaging. The plot is for the case $F_\ell=4$, $\mathrm{Re}_\ell=6400$ and for several times in the simulation, and displays the rapid increase in vertical shear anticipated from Fig. 2. Note that the mean square shear grows to a factor of over 30 of its original value. Furthermore, note

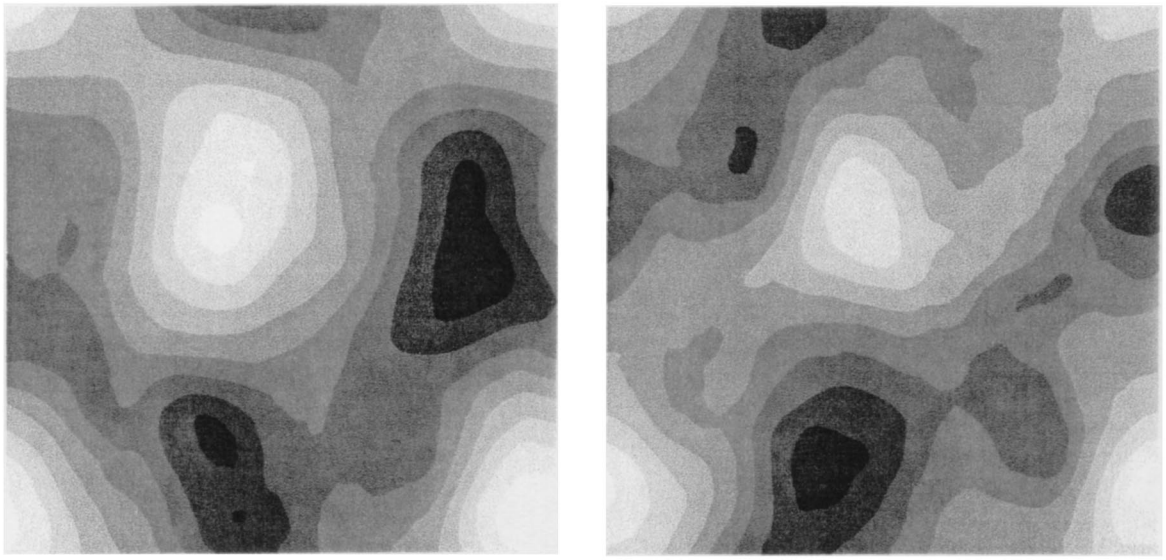

FIG. 2. Contour plots of the stream function ψ at $t=20$ and $z=2\pi\pm0.2\pi$ for the case with $F_\ell=4$, $\mathrm{Re}_\ell=3200$.

that the peak in the mean square shear ultimately occurs in regions of maximum mean square velocity (see Fig. 5 below), not in the regions where the shear was initially maximum. This is consistent with the heuristic arguments of Lilly[46] since, as the horizontal layers tend to decouple, the maximum shearing would be expected to occur in the regions of highest velocity. Finally, note that the mean square shear ultimately decays, since the overall flow field is continually decaying, as there is no source of energy.

The growth of the mean square shear is strongly dependent on the Reynolds number, as demonstrated in Fig. 4. In this figure the mean square shear is plotted versus z at $t=20$, which is approximately the time of maximum shear, for four cases at different Reynolds numbers, each with $F_\ell=4$. Note that each case was initiated with the same initial conditions; only the initial Reynolds number was changed. A monotonic increase in the mean square shear with increasing Reynolds number is observed. Furthermore, the maximum value for the case with $\mathrm{Re}_\ell=6400$ is observed to be more than four times larger than the case with $\mathrm{Re}_\ell=800$, and almost twice as large as the case with $\mathrm{Re}_\ell=3200$.

It is interesting to note that, although the mean square shear is growing rapidly during the first part of these simulations, the mean square horizontal velocity is continuously decaying. In Fig. 5 is plotted the horizontally averaged square of the horizontal velocity versus z for the same case as in Fig. 3. It is seen that the regions with larger mean square velocity remain localized vertically, and that the mean square velocity decays with time, as no source of energy is present.

The temporal behavior of the mean square horizontal velocity and its mean square vertical shear suggests that characteristic vertical length scales are decreasing with time. There are several vertical length scales of importance in this flow, ranging from the imposed scale ℓ down to the Kolmogorov scale (assuming the flow to be turbulent). Of particular relevance is the volume-averaged vertical Taylor scale ℓ_z, defined here as

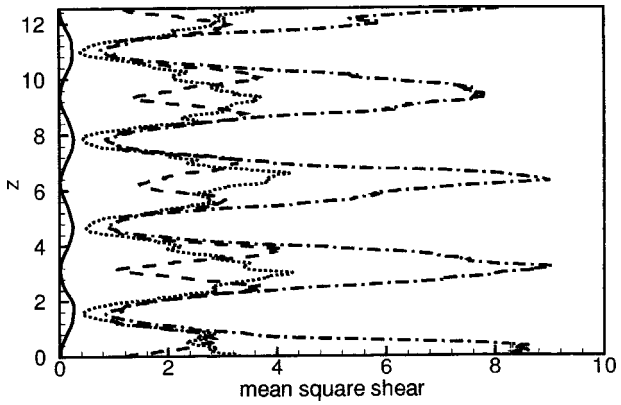

FIG. 3. Mean square vertical shearing of the horizontal velocity as a function of z for $F_\ell=4$ and $\mathrm{Re}_\ell=6400$ at different times: $t=0$ (—), 10 (---), 20 (-·-), and 30 (···).

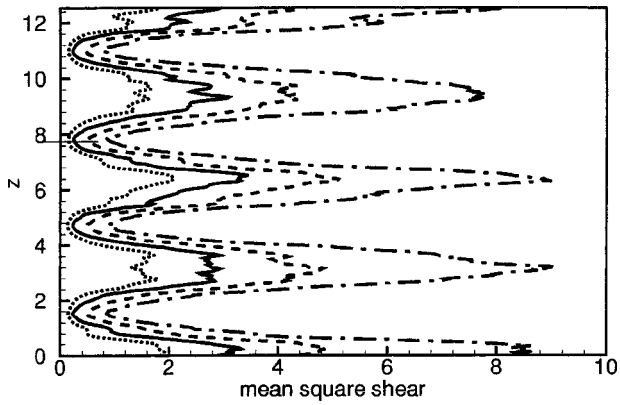

FIG. 4. Mean square vertical shearing of the horizontal velocity as a function of z for $F_\ell=4$ at $t=20$ for different Reynolds numbers: $\mathrm{Re}_\ell=800$ (···), 1600 (—), 3200 (---), and 6400 (-·-).

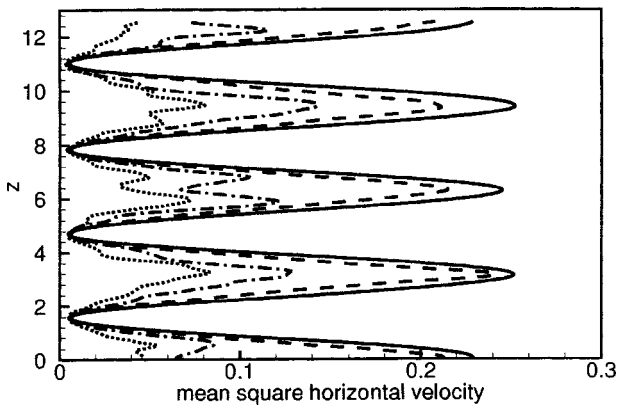

FIG. 5. Mean squared horizontal velocity vs z for $t=0$ (—), $t=10$ (---), $t=20$ (-·-), and $t=30$ (···), with $F_\ell=4$, $\mathrm{Re}_\ell=6400$.

$$\ell_z^2=\frac{\langle u^2+v^2\rangle}{\left\langle\left(\frac{\partial u}{\partial z}\right)^2+\left(\frac{\partial v}{\partial z}\right)^2\right\rangle}.$$

Here $\langle\cdot\rangle$ denotes the volume average of a quantity. One focus of this research is on whether the flow does become or remain turbulent, and some insight into this issue is gained by employing the gradient Richardson number, as discussed in the following. The vertical Taylor scale can enter into the definition of the gradient Richardson number. Furthermore, for turbulent flows the Taylor scale is closely related to the kinetic energy dissipation rate (see, e.g., Batchelor),[56] and therefore it is important in understanding flow energetics, and also estimates are readily available for it when making scaling arguments. For these reasons the vertical Taylor scale is the focus of the discussion on vertical length scales. In Fig. 6(a) the Taylor scale ℓ_z is plotted versus time for the same cases as in Fig. 4. The strong decrease in this differential scale can be observed, as well as its dependence on the Reynolds number.

The dependence of ℓ_z on the Reynolds number can be estimated, using the facts that, once the flows have developed turbulent-like behavior (beyond about $t=15$), both the horizontal components of the kinetic energy and the dissipation rate become approximately independent of the Reynolds number. (This can be seen in Figs. 13 and 16 below.) These facts suggest that the quantity

$$\frac{1}{\mathrm{Re}_\ell}\left\langle\left(\frac{\partial u}{\partial z}\right)^2+\left(\frac{\partial v}{\partial z}\right)^2\right\rangle=\frac{1}{\mathrm{Re}_\ell}\frac{\langle u^2+v^2\rangle}{\ell_z^2},\tag{2}$$

which is a part of the full dissipation-rate term, would be approximately independent of the Reynolds number as well. Therefore, the Reynolds number dependence of ℓ_z would be

$$\ell_z\sim\mathrm{Re}_\ell^{-1/2}.$$

This relationship is tested by plotting $\ell_z\,\mathrm{Re}_\ell^{1/2}$ versus time in Fig. 6(b); it is seen that, for times larger than about 15, the data from the simulations at different Reynolds numbers collapse fairly well. This gives strong support for the suggested dependence of ℓ_z on Re_ℓ, and also for the assumption that the term on the left-hand side of Eq. (2) becomes insensitive to the Reynolds number.

B. Flow instabilities

The strong growth of the mean square shear suggests that the Richardson number should be decreasing for these flow fields, and hence the potential for local instabilities and turbulence. Note that, for the Taylor–Green initial conditions (excluding the random noise), the minimum initial value of the Richardson number in the computational domain is

$$\mathrm{Ri}_{\min}(0)=\frac{N^2}{\left[\left(\frac{\partial u}{\partial z}\right)^2+\left(\frac{\partial v}{\partial z}\right)^2\right]_{\max}}=\left(\frac{2\pi}{F_\ell}\right)^2.$$

Therefore, for example, for the case with $F_\ell=4$, then $\mathrm{Ri}_{\min}(0)\approx 2.47$, implying that the entire flow field is initially

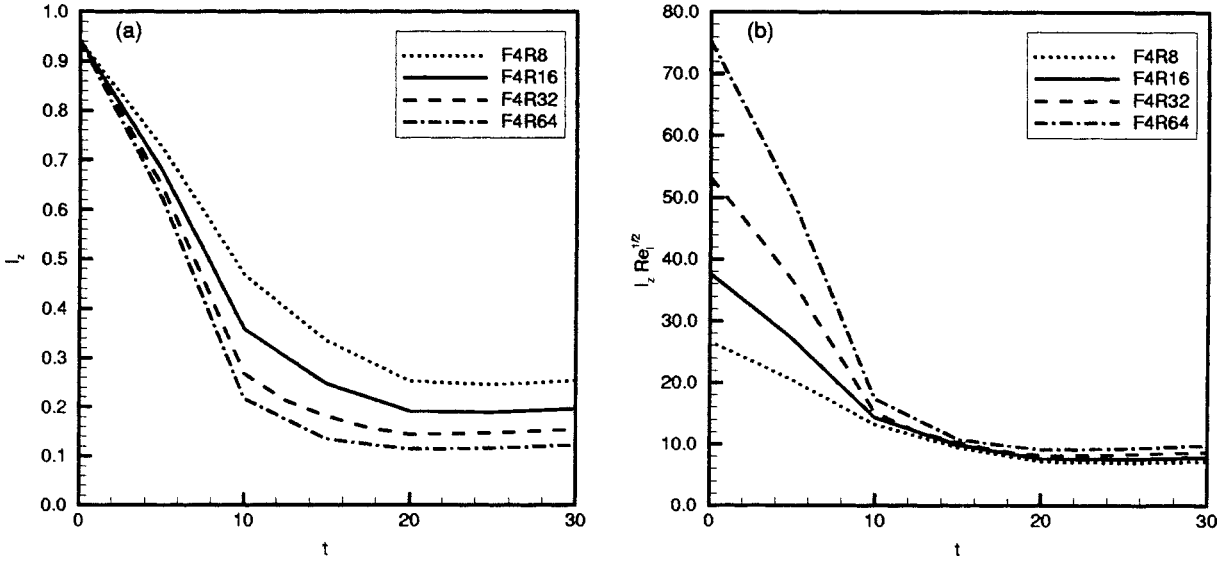

FIG. 6. (a) Vertical Taylor scale ℓ_z and (b) $\ell_z\,\mathrm{Re}_\ell^{1/2}$ vs time for different Reynolds numbers.

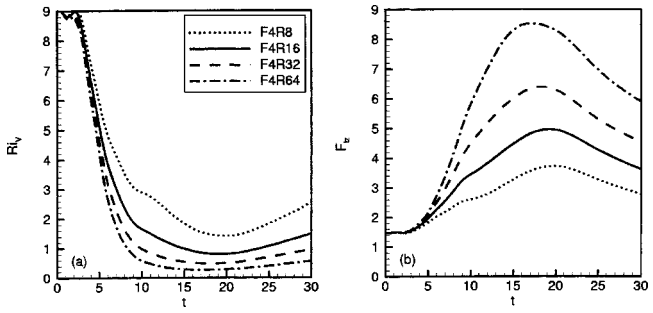

FIG. 7. (a) Volume-averaged Richardson number Ri_V and (b) Froude number based upon ℓ_z, both vs t, for four cases with $F_\ell=4$ and different values of Re_ℓ.

stable based upon a Richardson number criterion (which of course does not hold exactly for this unsteady, nonparallel flow). Furthermore, with the volume-averaged Richardson number defined here as

$$\mathrm{Ri}_V=\frac{N^2}{\left\langle\left(\frac{\partial u}{\partial z}\right)^2+\left(\frac{\partial v}{\partial z}\right)^2\right\rangle},$$

then for the initial Taylor–Green flow, $\mathrm{Ri}_V(0)=4\cdot\mathrm{Ri}_{\min}(0)$. For the case with $F_\ell=4$, then $\mathrm{Ri}_V(0)\approx 9.87$.

In Fig. 7 is plotted Ri_V vs t for the cases with $F_\ell=4$ and $\mathrm{Re}_\ell=800$, 1600, 3200, and 6400. It is seen that, in each case, this Richardson number drops rapidly to a value near 1 as the shear builds up. Furthermore, the values of Ri_V decrease as Re_ℓ is increased. It would be expected then that some local values of the Richardson number would be near or below 0 and local instabilities might develop.

It is often useful to consider a Froude number instead of the Richardson number. For example, in scaling arguments developed for the strongly stratified regime (e.g., Riley *et al.*,[25] Lilly,[46] Billand and Chomaz),[48] a Froude number based upon a vertical length scale is relevant. Such a Froude number can be defined by taking the vertical length scale to be the vertical Taylor scale ℓ_z, and by defining a horizontal root mean square velocity as $u'_H=\langle u^2\rangle^{1/2}=\langle v^2\rangle^{1/2}$; the relevant Froude number is then

$$F_{\ell_x}=\frac{2\pi u'_H}{N\ell_z}=\frac{2\pi}{\sqrt{2\,\mathrm{Ri}_V}},$$

where the definitions of ℓ_z and Ri_V above have been used. The Froude number F_{ℓ_z} is also plotted in Fig. 7. It starts from a value of about 1.4, and increases for each case as u'_H/ℓ_z increases. Significant variation with the Reynolds number is observed, consistent with the results for ℓ_z and Ri_V.

To address the issue of local instabilities suggested in Fig. 7, it is useful to examine the local Richardson number. Figure 8 contains gray-scale contour perspective plots of the local Richardson number at the time $t=20$ for two cases with $F_\ell=4$, i.e., $\mathrm{Re}_\ell=1600$ and 6400. This Richardson number is defined here as

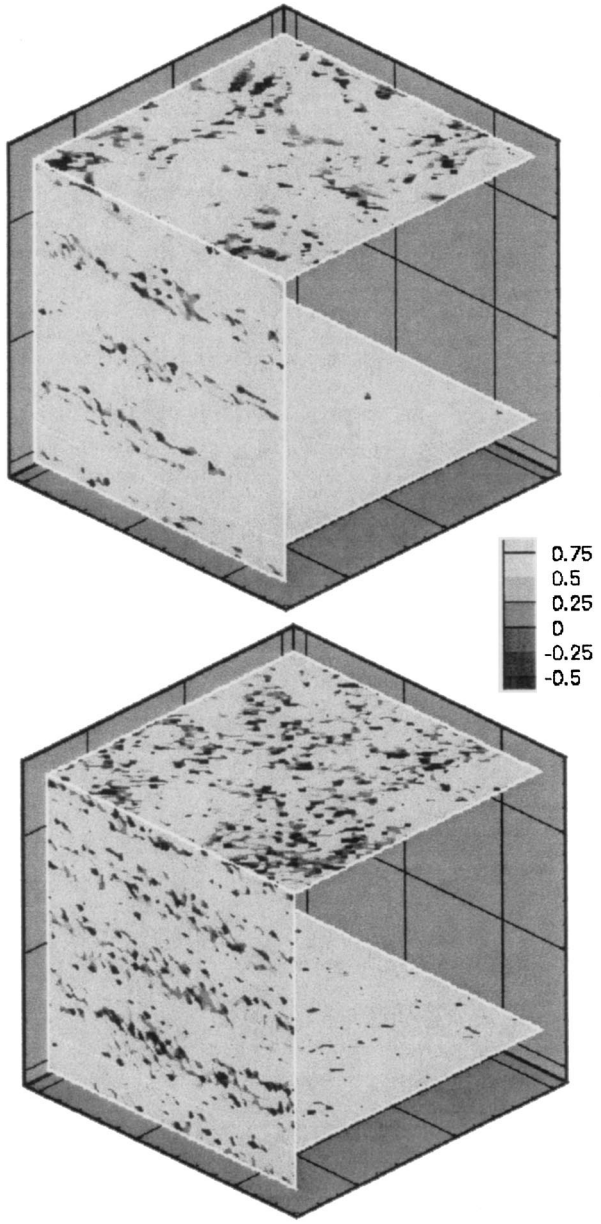

FIG. 8. Gray-scale contour perspective plots of the local Richardson number at $t=20$, $F_\ell=4$, for $\mathrm{Re}_\ell=1600$ (upper plot) and 6400 (lower plot).

$$\mathrm{Ri}=\frac{\frac{-g}{\rho_0}\frac{\partial\rho_T}{\partial z}}{\left(\frac{\partial u}{\partial z}\right)^2+\left(\frac{\partial v}{\partial z}\right)^2},$$

where $\rho_T(\mathbf{x},t)=\overline{\rho}(z)+\rho(\mathbf{x},t)$ is the sum of the ambient and fluctuating density fields, and ρ_0 is a reference density. Note that, as the gray scale indicates, darker regions correspond to the Richardson number being below 1/4 (and often below 0). Both cases show significant regions with low Richardson number, and that these regions occur in the layers with high shear. Two horizontal layers are displayed in each plot, one layer in a high shear and one in a low shear region. It is seen

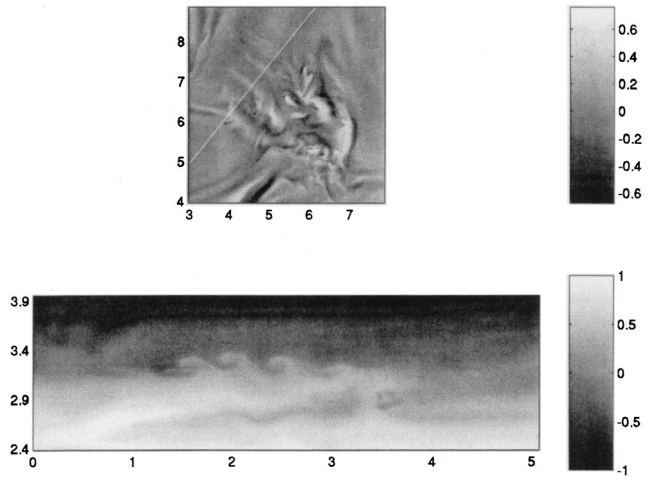

FIG. 9. Top panel shows part of a horizontal slice through the w field. The white dashed line gives the orientation of a vertical slice through the horizontal plane. The bottom panel shows ρ_T on that vertical slice. Both panels are for case F2R32.

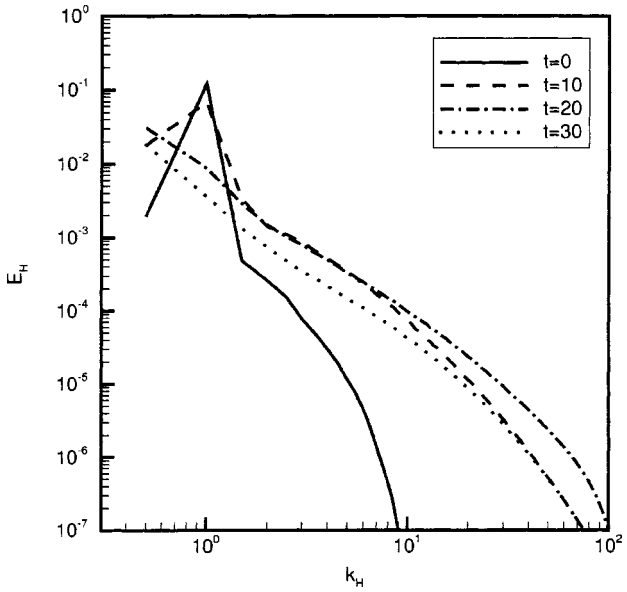

FIG. 10. Horizontal spectra of the horizontal velocity at four different times for the case with $F_\ell=4$, $\mathrm{Re}_\ell=6400$.

clearly that the occurrence of low Richardson numbers is localized in z, as expected from the plots of the mean square shear with z, Figs. 3 and 4.

It is found from further analyses of simulation results that, as the Reynolds number is increased, the regions of low and negative Richardson number become larger, occupying a larger volume of the computational domain. Furthermore, flow visualization reveals that the regions of low and negative Richardson number often have the appearance of Kelvin–Helmholtz instabilities or of turbulence. Unstable regions often start off in appearance as Kelvin–Helmholtz type ''rollers'' riding along high shear zones. For example, the top panel in Fig. 9 contains a gray-scale plot of a horizontal slice through a typical instability; in this case the vertical velocity w is plotted. In the bottom panel of Fig. 9 a vertical slice through this region has been taken; the vertical plane is oriented approximately perpendicular to the lines of constant w. Gray-scale contours of constant density are plotted in this plane, and Kelvin–Helmholtz-type ''rollers'' can be clearly seen. These rollers subsequently break down into three-dimensional, turbulent-like motion.

C. Flow energetics

Some idea of the nonlinear character of these flow fields can be obtained by examining the time development of $E_H(\kappa_H)$, the horizontal spectrum of the horizontal velocities, averaged over the vertical coordinate. A plot of this quantity is given in Fig. 10 for the case with $F_\ell=4$, $\mathrm{Re}_\ell=6400$. These spectra were obtained by summing the energy in circular shells in wave number space of width $\Delta\kappa_H=1$ for each horizontal plane, and then averaging the results in the vertical direction. The initial spike in the spectrum at $\kappa_H=1$ (the Taylor–Green scale) as well as the effect of the superimposed noise is evident at $t=0$. As the flow develops in time, energy is seen to flow upscale (to lower wave numbers), corresponding to the growth in the horizontal length scales noted in Figs. 1 and 2. Strong transfer of kinetic energy to smaller scales is also observed, as the energy spectra at high wave numbers rises in time; the energy at high wave numbers then ultimately decreases in time as the flow decays.

This same quantity is plotted in Fig. 11 at $t=20$ for the cases with $F_\ell=4$ and $\mathrm{Re}_\ell=800$, 1600, 3200, and 6400. The large-scale behavior is seen to be almost identical for each case, indicating some insensitivity of the energy-containing range to the Reynolds number. Clearly, however, the small-scale behavior is affected by the Reynolds number, with the smaller-scale energy increasing monotonically with the Reynolds number. Vertical spectra of the horizontal velocity were computed, and this same smaller-scale sensitivity to the

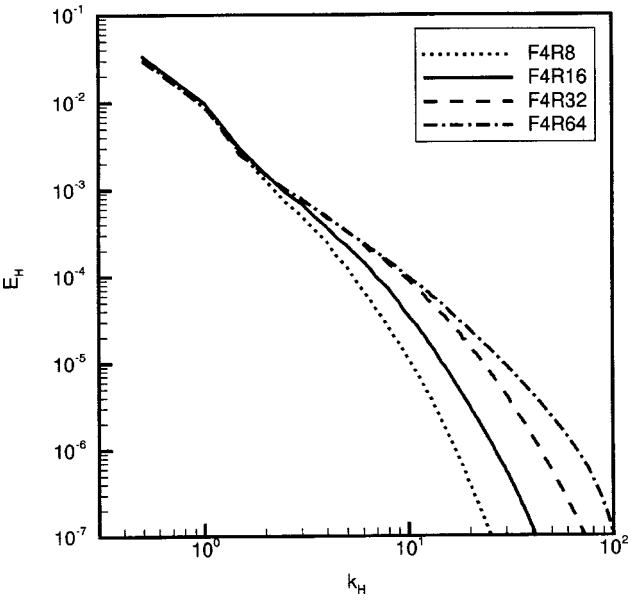

FIG. 11. Horizontal spectra of the horizontal velocity at $t=20$ for four cases with $F_\ell=4$ and different values of Re_ℓ.

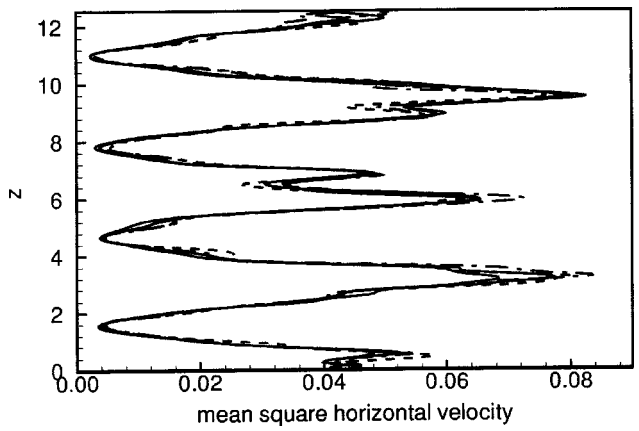

FIG. 12. Mean squared velocity vs z at $t=30$, $F_\ell=4$, and $\mathrm{Re}_\ell=800$ (···), $\mathrm{Re}_\ell=1600$ (—), $\mathrm{Re}_\ell=3200$ (---), and $\mathrm{Re}_\ell=6400$ (-·-).

Reynolds number observed, consistent also with the sensitivity of the mean square shear to the Reynolds number (Fig. 4).

This insensitivity of the large scale motions to the Reynolds number can also be seen in the behavior of the horizontal average of the square of the horizontal velocity with z. In Fig. 12 is such a plot, at $t=30$, for the same cases as for Fig. 11. We find here that, although there is a significant difference in the behavior of the mean square shear with z for different Reynolds numbers (see Fig. 4), very little difference can be detected in the mean square velocity.

The overall behavior of the horizontal components of the kinetic energy can be seen in Fig. 13, in which the volume average of this quantity is plotted versus t for the cases $F_\ell=4$, and $\mathrm{Re}_\ell=800$, 1600, 3200, and 6400. The overall decay is not affected much by changes in the Reynolds number, as the decay is being controlled by the large-scale dynamics. The oscillations in the kinetic energy appearing especially at the earlier-times are due to both the cyclostrophic adjustment of the density and pressure fields to the Taylor–Green initial

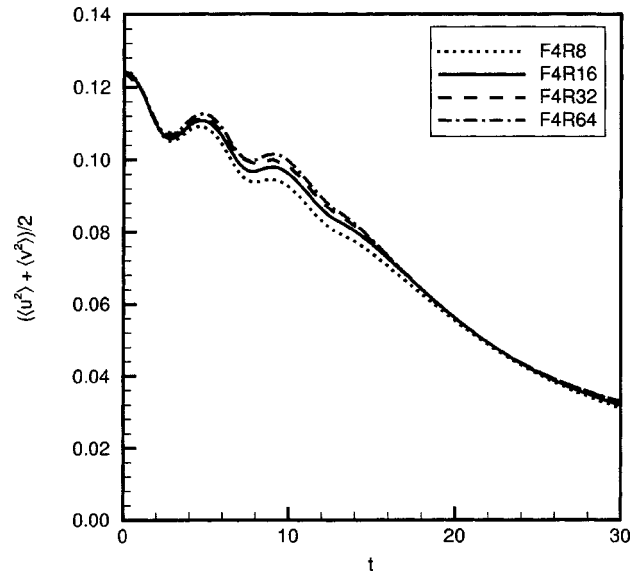

FIG. 13. Volume-averaged horizontal components of the kinetic energy vs time with $F_\ell=4$ and different values of Re_ℓ.

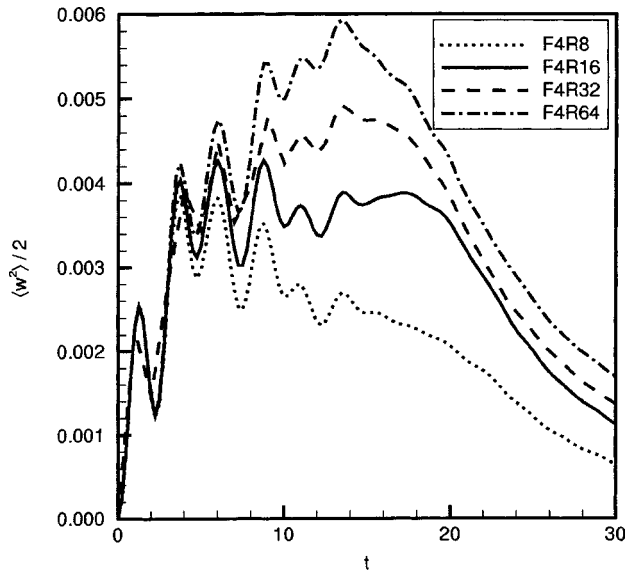

FIG. 14. Volume-averaged vertical component of the kinetic energy vs time with $F_\ell=4$ and different values of Re_ℓ.

conditions as well as to the generation of internal waves. Again note that the nondimensional buoyancy period for these flows is $(2\pi/N)/(\ell/\mathcal{U})=4$.

In Fig. 14 is plotted the time development of the volume-averaged, vertical component of the kinetic energy for the same cases as in Fig. 13 (note the difference in the scaling in the plots). Clearly this component of the kinetic energy is much smaller than the horizontal components (for example, its value at $t=20$ is about 15% of the value of either of the horizontal components), as the flow remains dominated by the vortical mode component. Some oscillations in this component of the kinetic energy are observed, probably due both to internal waves excited by the developing flow field, and to motions along constant density (isopycnal) surfaces tilted out of the horizontal by cyclostrophic adjustment. Finally, there is a discernible increase in $(1/2)\langle w^2\rangle$ as the Reynolds number is increased. This appears to be due to the increased generation of instabilities and turbulent-like motions as the Reynolds number is increased.

In Fig. 15 are plots of the volume-averaged potential energy versus time for the same cases as in the previous two figures. The (nondimensional) potential energy is defined here as (see, e.g., Gill[57] for a detailed discussion of potential energy)

$$\mathrm{PE}=\frac{1}{2}\left(\frac{2\pi}{F_\ell}\right)^2\rho^2.$$

Note that the value of the potential energy is significantly larger that of $(1/2)\langle w^2\rangle$ due to the cyclostrophic adjustment of the density field. There are also wave-like oscillations corresponding to those observed in the kinetic energy. As with $(1/2)\langle w^2\rangle$, there is a discernible increase in the potential energy as the Reynolds number is increased, presumably due to the increase in small-scale instabilities and turbulent-like motions.

In completing the picture of the energetics of these flows, it is useful to examine the energy dissipation rates. In

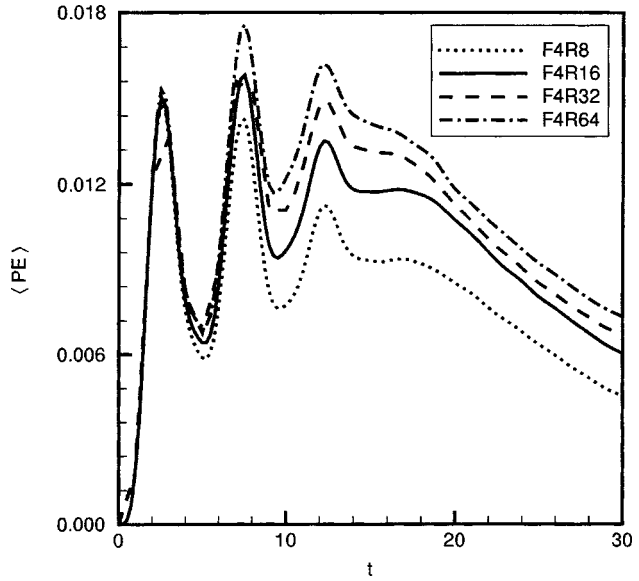

FIG. 15. Volume-averaged potential energy vs time with $F_\ell = 4$ and different values of Re_ℓ.

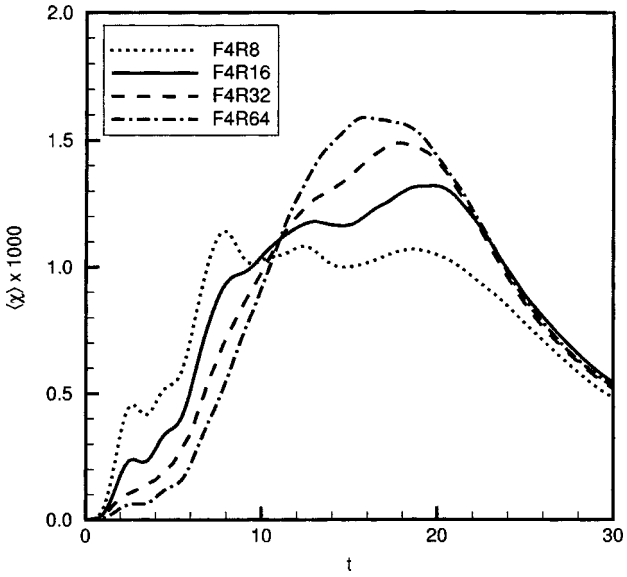

FIG. 17. Volume-averaged potential energy dissipation rate vs time with $F_\ell = 4$ and different values of Re_ℓ.

Fig. 16 is plotted the volume-averaged kinetic energy dissipation rate, $\langle \epsilon \rangle$, versus time for the cases with $F_\ell = 4$, and $\mathrm{Re}_\ell = 800$, 1600, 3200, and 6400. Since the initial conditions are identical for each of these simulations, and only the Reynolds number is changed, then the initial dissipation rate should be inversely proportional to the Reynolds number, as observed in Fig. 16. As the shearing rapidly increases and small-scale instabilities occur, however, the trend is reversed and the kinetic energy dissipation rates are seen to increase with Reynolds number. Finally, as the dissipation rates begin to decay, with the dynamics being controlled by the approximately inviscid larger-scale motions, the dissipation rates become somewhat insensitive to the Reynolds number.

In Fig. 17 is given the volume-averaged potential energy dissipation rate $\langle \chi \rangle$ versus time for the same cases as in Fig. 16. Here the (nondimensional) potential energy dissipation rate is defined as

$$\chi = \frac{1}{\mathrm{Re}_\ell \mathrm{Pr}} \left(\frac{2\pi}{F_\ell} \right)^2 \nabla \rho \cdot \nabla \rho.$$

Since there are initially no density fluctuations, the potential energy dissipation rate is initially zero. For early times, $\langle \chi \rangle$ is approximately inversely proportional to the Reynolds number (recall that the Prandtl number is the same for all cases), for the same reasons as for $\langle \epsilon \rangle$. As the flows evolve, the values of $\langle \chi \rangle$ remain significantly lower than those of $\langle \epsilon \rangle$, for example $\langle \chi \rangle / \langle \epsilon \rangle \approx 0.43$ at $t = 20$ for the case with $\mathrm{Re}_\ell = 6400$. As with $\langle \epsilon \rangle$, $\langle \chi \rangle$ tends to be somewhat insensitive to the Reynolds number as the flows decay.

The quantity $\Gamma = \langle \chi \rangle / \langle \epsilon \rangle$ represents the ratio of the rate of irreversible loss of potential energy to the background density field to the rate of irreversible loss of kinetic energy to internal energy. This ratio (or sometimes the ratio of the time-integrated values of each) is often called the mixing efficiency, the efficiency with which the flow mixes the density field at the molecular level. Figure 18 is a plot of Γ versus time for the four cases with $F_\ell = 4$. Note that in the early stages of the flows, values of Γ well above 0.5 are achieved. As the flows become unstable and patches of turbulent-like motions develop, the ratio settles down to a value of a little above 0.4, with some weak dependence on the Reynolds number. Both the larger values of Γ in the pre-turbulence regime and the leveling off to values near 0.4 (for $\mathrm{Pr} = 1.0$) are consistent with other numerical simulations of stratified turbulent flow (see, e.g., Smyth *et al.*[58] and Staquet[59]).

A final point regarding energy dissipation is the contribution of the vertical shearing of the horizontal motion, i.e.,

$$\mathcal{S} = \nu \left\langle \left(\frac{\partial u}{\partial z} \right)^2 + \left(\frac{\partial v}{\partial z} \right)^2 \right\rangle,$$

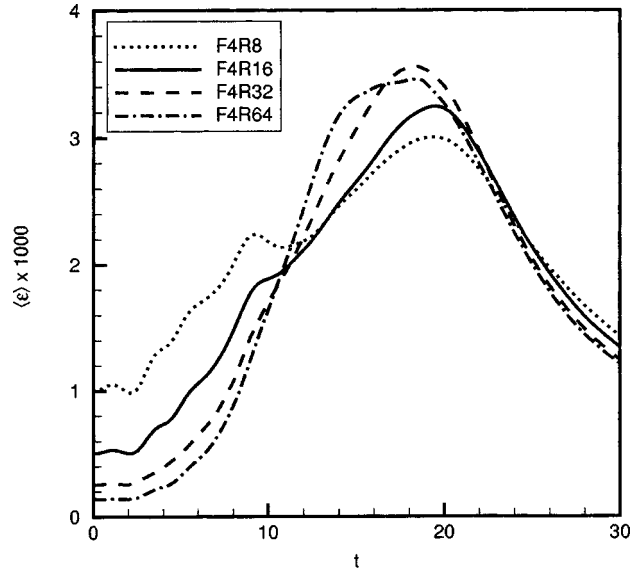

FIG. 16. Volume-averaged kinetic energy dissipation rate vs time with $F_\ell = 4$ and different values of Re_ℓ.

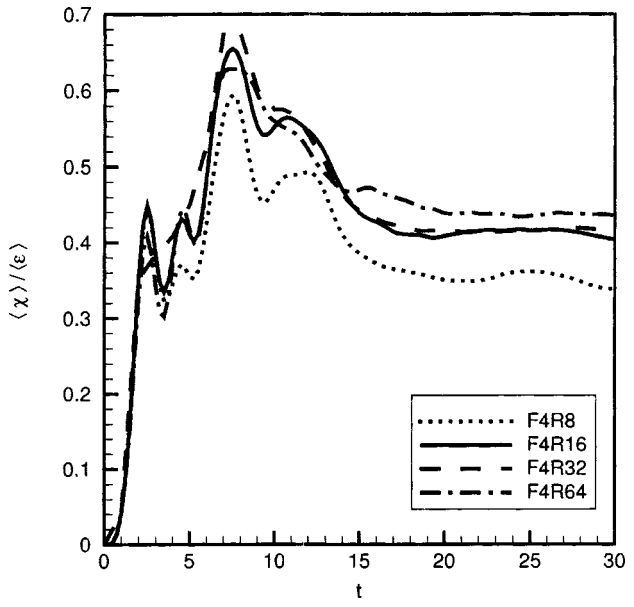

FIG. 18. The mixing efficiency Γ vs time with $F_\ell = 4$ and different values of Re_ℓ.

to the total kinetic energy dissipation rate $\langle \epsilon \rangle$. The results of Fincham *et al.*[24] indicate that, in the late wake of a grid, this component accounts for about 80% of the kinetic energy dissipation rate, i.e., $\mathcal{S}/\langle \epsilon \rangle \approx 0.8$. Further analysis of the present simulation results indicates that this ratio is a strong function of the Reynolds number. For the highest Reynolds number case ($\mathrm{Re}_\ell = 6400$), the ratio is approximately 0.412, not far from the value for isotropic turbulence of 0.323 (see, e.g., Hinze[60]). As the Reynolds number is decreased and hence the tendency for instability and turbulent-like motions decreases, this ratio increases, and is approximately 0.725 for the case with $\mathrm{Re}_\ell = 800$.

IV. CONCLUSIONS

Simulations were carried out for flows initialized with quasi-horizontal motions at Froude numbers of order 1, so that the effect of the ambient density stratification was initially strong and vertical motions were somewhat inhibited. These conditions are intended to be a simplified model for the quasi-horizontal motions observed when the Froude number is of order 1 in various laboratory flows and numerical simulations. Specifically, the initial velocity field consisted of Taylor–Green vortices with noise superimposed, and simulations were performed for a range of initial Reynolds numbers in order to determine the overall flow dynamics, including the effects of the Reynolds number.

It is found that, with the vertical motions moderately inhibited, there is a strong tendency for horizontal length scales to grow, reminiscent of two-dimensional turbulence. At the same time, however, there is a strong tendency for vertical scales to decrease and the vertical shearing of the horizontal motions to increase. This increase of the vertical shear is possibly due to the mechanism suggested by Lilly,[46] whereby the motions in adjacent horizontal layers become to some extent uncoupled. The flows are initiated at a Richardson number somewhat above 1; the growth of the shear continues until the local Richardson numbers become of order 1, at which point local instabilities and turbulent-like motions appear.

The overall flow dynamics appear to be only mildly sensitive to the Reynolds number, as the larger-scale, quasi-horizontal motions evolve almost inviscidly while transferring energy to the smaller-scale motions. Analogous to Kolmogorov's ideas for high Reynolds number, fully three-dimensional turbulence, the smaller-scale motions respond to the energy transfer with an increase in the local strain rates until the same dissipation rates are ultimately achieved for the different Reynolds number cases. These results then suggest the possibility of an inertial range at higher wave numbers. There is a $k^{-5/3}$ behavior over almost one decade in the plot of the horizontal spectra of the horizontal velocity given in Fig. 10 at $t = 20$, hinting at an inertial range, but much higher Reynolds number simulations would be required to verify the presence of such a range.

These simulations do not address the fundamental question of whether the quasi-horizontal motions observed in the laboratory experiments would also occur at the high Reynolds numbers typical of turbulence in the atmosphere and the oceans. They do suggest, however, that if the vortices are formed at small enough atmospheric or oceanic scales that rotational effects are unimportant, then the dynamics on the laboratory scale would be similar to those at atmospheric and oceanic scales (not considering other effects such as ambient current shear and variability in density stratification). Furthermore, they imply that, if the vortices develop, they could be a continuing source of smaller-scale turbulence. Finally, the results suggest that large-eddy simulation could be effective in treating these motions, assuming that the subgrid-scale modeling could mimic the appropriate energy transfer rates to the subgrid scales from the larger-scale, quasi-horizontal motions, a transfer process which may be significantly different from that of more classical turbulent flows.

Regarding the generation of the vortices from initially three-dimensional turbulence at high Reynolds numbers, the results suggest that, as a high Reynolds number flow decays so that the Froude number becomes of order 1, the generation of vertical shearing would continually occur, along with the local instabilities and smaller-scale turbulence. The Froude number based upon an appropriate vertical length scale (for example, the Taylor scale ℓ_z), say F_v, would become and remain of order 1 until the Reynolds number of the flow had also decreased to order 1. At this point the generation of shear would be inhibited by viscosity, and F_v would decrease below 1, as in the laboratory experiments (e.g., Spedding[61]) and numerical simulations (e.g., Métais and Herring[38]). What is not clear is whether, at high Reynolds numbers, the larger horizontal-scale motions would grow in scale and maintain sufficient vertical coherence to be identified as coherent vortices similar to those observed in the laboratory.

Using these results and the heuristic argument of Lilly,[46] it is possible to estimate the Reynolds number below which the flow would not become or remain turbulent. To do this it is convenient to work with dimensional variables; in this

discussion, all the variables will be assumed to be dimensional. Lilly suggested that strong stratification would lead to increasing vertical shearing of the horizontal motions, until local shear instabilities develop. This implies that a local Richardson number is useful in establishing a criterion for instability and turbulence.

Consider again the local gradient Richardson number,

$$\mathrm{Ri}=\frac{\frac{-g}{\rho_0}\frac{\partial \rho_T}{\partial z}}{\left(\frac{\partial u}{\partial z}\right)^2+\left(\frac{\partial v}{\partial z}\right)^2},$$

and take the (constant) buoyancy frequency squared N^2 as the estimate for the numerator. To estimate the denominator, assume that

$$\nu\left[\left(\frac{\partial u}{\partial z}\right)^2+\left(\frac{\partial v}{\partial z}\right)^2\right],$$

principal terms in the kinetic energy dissipation rate ϵ, can be estimated by ϵ. Furthermore, assume that ϵ is of the order of the time rate-of-change term in the kinetic energy equation. Therefore,

$$\frac{\partial}{\partial t}\frac{1}{2}|\mathbf{u}|^2\sim\epsilon\sim\nu\left[\left(\frac{\partial u}{\partial z}\right)^2+\left(\frac{\partial v}{\partial z}\right)^2\right].$$

To estimate the time rate-of-change term, use u_H', the root mean square horizontal component of the velocity, and ℓ_H, a horizontal scale of the energy-containing motions. Assuming that time scales as the horizontal advective time ℓ_H/u_H', then

$$\frac{\partial}{\partial t}\frac{1}{2}|\mathbf{u}|^2\sim\frac{{u_H'}^3}{\ell_H}$$

and thus

$$\left[\left(\frac{\partial u}{\partial z}\right)^2+\left(\frac{\partial v}{\partial z}\right)^2\right]\sim\frac{1}{\nu}\frac{{u_H'}^3}{\ell_H}.$$

Therefore the Richardson number scales as, approximately,

$$\frac{N^2}{\left(\frac{1}{\nu}\frac{{u_H'}^3}{\ell_H}\right)}=\frac{N^2\ell_H^2}{{u_H'}^2}\frac{\nu}{u_H'\ell_H}=\frac{1}{F_{\ell_H}^2}\frac{1}{\mathrm{Re}_{\ell_H}},$$

where the local Froude and Reynolds numbers are defined by

$$F_{\ell_H}=\frac{u_H'}{N\ell_H},\quad \mathrm{Re}_{\ell_H}=\frac{u_H'\ell_H}{\nu}.$$

Applying the Richardson number criterion, the flow will become or remain turbulent if, approximately,

$$\mathrm{Ri}<1,$$

or if

$$\mathrm{Re}_{\ell_H}>\frac{1}{F_{\ell_H}^2}.$$

This result suggests a strong dependence of the critical Reynolds number on the stratification.

A similar result was obtained by Billant and Chomaz[48] for estimating when viscous effects become important in strongly stratified flows. Assuming, from a detailed scaling analysis, that a Froude number based upon a vertical scale is of order 1, and defining a Reynolds number based upon the usual ratio of inertial to viscous forces, they found that viscous effects will be important when $\mathrm{Re}_{\ell_H}<1/F_{\ell_H}^2$. Clearly the criterion for when viscous forces become important is related to that at which turbulence cannot exist.

The vertical differential scale ℓ_z evolves based upon the local fluid dynamics, and not so much on the initial vertical scale ℓ. Furthermore, because a Froude number based upon the vertical scale has been often used in scaling analysis, it is useful to determine the dependence of this Froude number on other important parameters. Since, by definition,

$$\frac{2u_H'^2}{\ell_z^2}=\left\langle\left(\frac{\partial u}{\partial z}\right)^2+\left(\frac{\partial v}{\partial z}\right)^2\right\rangle,$$

then, from the scaling arguments given above,

$$\ell_z\sim\left(\frac{\nu\ell_H}{u_H'}\right)^{1/2}.$$

Therefore,

$$F_{\ell_z}=\frac{u_H'}{N\ell_z}\sim\frac{u_H'}{N\left(\frac{\nu\ell_H}{u_H'}\right)^{1/2}}=F_{\ell_H}\mathrm{Re}_{\ell_H}^{1/2}.$$

Note that for large Reynolds number Re_{ℓ_H}, F_{ℓ_z} is much larger than F_{ℓ_H}, and F_{ℓ_z} may not be small even though F_{ℓ_H} is small. But for $\mathrm{Re}_{\ell_H}\sim1$, then $F_{\ell_z}\sim F_{\ell_H}$. In laboratory experiments and numerical simulations in which the Reynolds number based upon ℓ_H is not large, then if F_{ℓ_H} is small, F_{ℓ_z} would also be expected to be small. This may explain why the scaling based upon F_{ℓ_z} appears to be useful in describing the dynamics of the late stages of decay in the laboratory experiments (e.g., Spedding[61]) and numerical simulations (e.g., Métais and Herring[38]).

ACKNOWLEDGMENTS

This research is funded by the U.S. Office of Naval Research, Grant No. N00014-00-1-0752, managed by Dr. L. Patrick Purtell; grants of high performance computer (HPC) time were provided by the Arctic Region Supercomputing Center and the Army HPC Research Center. The authors would like to thank Kraig Winters for very helpful discussions of the results.

[1] O. Andreassen, P. O. Hvidsten, D. C. Fritts, and S. Arendt, "Vorticity dynamics in a breaking internal gravity wave. 1. Initial instability evolution," J. Fluid Mech. **367**, 27 (1998).
[2] M.-P. Lelong and T. J. Dunkerton, "Inertia-gravity wave breaking in three dimensions. I. Convectively stable waves," J. Atmos. Sci. **15**, 2473 (1998).
[3] M.-P. Lelong and T. J. Dunkerton, "Inertia-gravity wave breaking in three dimensions. II. Convectively unstable waves," J. Atmos. Sci. **15**, 2489 (1998).
[4] P. N. Lombard and J. J. Riley, "Instability and breakdown of internal gravity waves. I. Linear stability analysis," Phys. Fluids **8**, 3271 (1996).
[5] P. N. Lombard and J. J. Riley, "On the breakdown into turbulence of

propagating internal waves,'' Dyn. Atmos. Oceans **23**, 345 (1996).
[6]P. Bouruet-Aubertot, J. Sommeria, and C. Staquet, ''Breaking of standing internal gravity waves through two-dimensional instabilities,'' J. Fluid Mech. **285**, 265 (1995).
[7]I. Orlanski and K. Bryan, ''Formation of thermocline step structure by large-amplitude internal gravity waves,'' J. Geophys. Res. **74**, 6975 (1969).
[8]J. S. Turner, *Buoyancy Effects in Fluids* (Cambridge University Press, New York, 1973).
[9]W. D. Smyth, ''Dissipation-range geometry and scalar spectra in sheared stratified turbulence,'' J. Fluid Mech. **401**, 209 (1999).
[10]J. J. Riley and M.-P. Lelong, ''Fluid motions in the presence of strong stable stratification,'' Annu. Rev. Fluid Mech. **32**, 613 (2000).
[11]G. R. Spedding, F. K. Browand, and A. M. Fincham, ''The long-time evolution of the initially-turbulent wake of a sphere in a stable stratification,'' Dyn. Atmos. Oceans **23**, 171 (1996).
[12]G. R. Spedding, F. K. Browand, and A. M. Fincham, ''Turbulence, similarity scaling and vortex geometry in the wake of a towed sphere in a stably stratified fluid,'' J. Fluid Mech. **314**, 53 (1996).
[13]J.-T. Lin and Y.-H. Pao, ''Wakes in stratified fluids: A review,'' Annu. Rev. Fluid Mech. **11**, 317 (1979).
[14]J.-M. Chomaz, P. Bonneton, A. Butet, and E. J. Hopfinger, ''Vertical diffusion of the far wake of a sphere moving in a stratified fluid,'' Phys. Fluids A **5**, 2799 (1993).
[15]M. Bonnier, O. Eif, and P. Bonneton, ''On the density structure of far-wake vortices in a stratified fluid,'' Dyn. Atmos. Oceans **31**, 117 (2000).
[16]M. Bonnier and O. Eiff, ''Experimental investigation of the collapse of a turbulent wake in a stably stratified fluid,'' Phys. Fluids **14**, 791 (2002).
[17]J. B. Flór and G. J. F. van Heijst, ''Experimental study of dipolar vortex structures in a stratified fluid,'' J. Fluid Mech. **279**, 101 (1994).
[18]S. I. Voropayev, Y. D. Afanasyev, and I. A. Filippov, ''Horizontal jet and vortex dipoles in a stratified medium,'' J. Fluid Mech. **227**, 543 (1991).
[19]S. I. Voropayev, Z. Zhang, D. L. Boyer, H. J. S. Fernando, and C. W. Pok, ''Horizontal jets in a rotating stratified fluid,'' Phys. Fluids **9**, 115 (1997).
[20]S. I. Voropayev, S. A. Smirnov, and A. Brandt, ''Dipolar eddies in a stratified shear flow,'' Phys. Fluids **13**, 3820 (2001).
[21]R. R. Trieling and G. J. F. van Heijst, ''Decay of monopolar vortices in a stratified fluid,'' Fluid Dyn. Res. **23**, 735 (1998).
[22]M. Beckers, R. Verzicco, H. J. H. Clercx, and G. J. F. van Heijst, ''Dynamics of pancake-like vortices in a stratified fluid: Experiments, theory and numerical simulations,'' J. Fluid Mech. **433**, 1 (2001).
[23]M. Beckers M, H. J. H. Clerx, G. J. F. van Heijst, and R. Verzicco, ''Dipole formation by two interacting shielded monopoles in a stratified fluid,'' Phys. Fluids **14**, 704 (2002).
[24]A. M. Fincham, T. Maxworthy, and G. R. Spedding, ''Energy dissipation and vortex structure in freely-decaying, stratified grid turbulence,'' Dyn. Atmos. Oceans **23**, 155 (1996).
[25]J. J. Riley, R. W. Metcalfe, and M. A. Weissman, ''Direct numerical simulations of homogeneous turbulence in density stratified fluids,'' in *Proceedings of the AIP Conference on Nonlinear Properties of Internal Waves* (AIP, Woodbury, 1981), pp. 79–112.
[26]J. C. McWilliams, ''A uniformly valid model spanning the regimes of geostrophic and isotropic, stratified turbulence: balanced turbulence,'' J. Atmos. Sci. **42**, 1773 (1985).
[27]M.-P. Lelong and J. J. Riley, ''Internal wave–vortical mode interactions in strongly stratified flows,'' J. Fluid Mech. **232**, 1 (1991).
[28]P. Bartello, ''Geostrophic adjustment and inverse cascades in rotating stratified turbulence,'' J. Atmos. Sci. **52**, 4410 (1995).
[29]A. J. Majda and P. F. Embid, ''Averaging over fast gravity waves for geophysical flows with unbalanced initial data,'' Theor. Comput. Fluid Dyn. **11**, 155 (1998).
[30]P. F. Embid and A. J. Majda, ''Averaging over fast gravity waves for geophysical flows with arbitrary potential vorticity,'' Commun. Partial Differ. Equ. **21**, 619 (1996).
[31]T. Warn, ''Statistical mechanical equilibria of the shallow water equations,'' Tellus, Ser. A **38A**, 1 (1986).
[32]R. Plougonven and V. Zeitlin, ''Internal gravity wave emission from a pancake vortex: An example of wave-vortex interaction in strongly stratified flows,'' Phys. Fluids **14**, 1259 (2002).
[33]A. Babin, A. Mahalov, B. Nicolaenko, and Y. Zhou, ''On the asymptotic regimes and the strongly stratified limit of rotating Boussinesq equations,'' Theor. Comput. Fluid Dyn. **9**, 223 (1997).
[34]P. Bartello, ''Potential vorticity, resonance and dissipation in rotating convective turbulence,'' *Geophysical and Astrophysical Convection*, edited by R. H. Kerr, P. Fox, and C.-H. Moeng (Gordon and Breach, New York, 1999).
[35]F. S. Godeferd and C. Cambon, ''Detailed investigation of energy transfers in homogeneous stratified turbulence,'' Phys. Fluids **6**, 2084 (1994).
[36]H. Hanazaki and J. C. R. Hunt, ''Linear processes in unsteady, stably stratified turbulence,'' J. Fluid Mech. **318**, 303 (1996).
[37]J. R. Herring and O. Métais, ''Numerical experiments in forced stably stratified turbulence,'' J. Fluid Mech. **202**, 97 (1989).
[38]O. Métais and J. R. Herring, ''Numerical simulations of freely evolving turbulence in stably stratified fluids,'' J. Fluid Mech. **202**, 117 (1989).
[39]T. Gerz and H. Yamazaki, ''Direct numerical simulations of buoyancy driven turbulence in stably stratified fluid,'' J. Fluid Mech. **249**, 415 (1993).
[40]D. Ramsden and G. Holloway, ''Energy transfers across an internal wave-vortical mode spectrum,'' J. Geophys. Res., [Oceans] **97**, 3659 (1992).
[41]T. Gerz, U. Schumann, and S. E. Elghobashi, ''Direct numerical simulation of statified homogeneous turbulent shear flows,'' J. Fluid Mech. **200**, 563 (1989).
[42]S. E. Holt, J. R. Koseff, and J. H. Ferziger, ''A numerical study of the evolution and structure of homogeneous stably stratified sheared turbulence,'' J. Fluid Mech. **237**, 499 (1992).
[43]F. G. Jacobitz, S. Sarkar, and C. W. van Atta, ''Direct numerical simulations of the turbulence evolution in a uniformly sheared and stably stratified flow,'' J. Fluid Mech. **342**, 231 (1997).
[44]Y. Kimura and J. R. Herring, ''Diffusion in stably-stratified turbulence,'' J. Fluid Mech. **328**, 253 (1996).
[45]M. J. Gourlay, S. C. Arendt, D. C. Fritts, and J. Werne, ''Numerical modeling of initially turbulent wakes with net momentum,'' Phys. Fluids **13**, 3783 (2001).
[46]D. K. Lilly, ''Stratified turbulence and the mesoscale variability of the atmosphere,'' J. Atmos. Sci. **40**, 749 (1983).
[47]P. Billant and J.-M. Chomaz, ''Three-dimensional stability of a columnar vortex pair in a stratified fluid,'' J. Fluid Mech. **419**, 65 (2000).
[48]P. Billant and J.-M. Chomaz, ''Self-similarity of strongly stratified inviscid flows,'' Phys. Fluids **13**, 1645 (2001).
[49]G. I. Taylor and A. E. Green, ''Mechanisms of the production of small eddies from large ones,'' Proc. R. Soc. London, Ser. A **158**, 499 (1937).
[50]O. M. Phillips, *The Dynamics of the Upper Ocean* (Cambridge University Press, Cambridge, 1966).
[51]C. Staquet and J. J. Riley, ''On the velocity field associated with potential vorticity,'' Dyn. Atmos. Oceans **14**, 93 (1989).
[52]M. E. Brachet, D. I. Meiron, S. A. Orszag, B. G. Nickel, R. H. Morf, and U. Frisch, ''Small scale structure of the Taylor–Green vortex,'' J. Fluid Mech. **130**, 411 (1983).
[53]J. J. Riley, M.-P. Lelong, and D. N. Slinn, ''Organized structures in strongly stratified flows,'' in *Turbulence and Coherent Structures*, edited by O. Métais and M. Lesieur (Kluwer Academic, Dordrecht, 1991), pp. 413–428.
[54]S. A. Orszag and G. S. Patterson, Jr., ''Numerical simulation of turbulence,'' in *Statistical Models and Turbulence*, edited by J. Ehlers, K. Hepp, and H. A. Weidenmüller (Springer, New York, 1972), pp. 127–147.
[55]R. M. Kerr, ''Higher-order derivative correlations and the alignment of small-scale structures in isotropic numerical turbulence,'' J. Fluid Mech. **153**, 31 (1985).
[56]G. K. Batchelor, *The Theory of Homogeneous Turbulence* (Cambridge University Press, Cambridge, 1953).
[57]A. E. Gill, *Atmosphere-Ocean Dynamics* (Academic, New York, 1982).
[58]W. D. Smyth, J. N. Moum, and D. R. Caldwell, ''The efficiency of mixing in turbulent patches: Inferences from direct simulations and microstructure observations,'' J. Phys. Oceanogr. **31**, 1969 (2001).
[59]C. Staquet, ''Mixing in a stably-stratified shear layer: Two- and three-dimensional numerical experiments,'' Fluid Dyn. Res. **27**, 367 (2000).
[60]J. O. Hinze, *Turbulence* (McGraw–Hill, New York, 1975).
[61]G. R. Spedding, ''Vertical structure in stratified wakes at high initial Froude number,'' J. Fluid Mech. **454**, 71 (2002).